ACKNOWLEDGMENT

The work was supported by Scientific Research Grant from Ministry of Education, No. 225369.

LITERATURE CITED

de Boer, J. H., "The dynamic Character of Adsorption," Oxford (1953).
Carman, P. C., "Fluid Flow Through Granular Beds," *Trans. Inst. Chem. Eng.*, **15**, 150 (1973).
Gilliland, E. R., R. F. Baddour,G. P. Perkinson and K. J. Sladek, "Diffusion on Surfaces. I. Effect of Concentration on the Diffusivity of Physically Adsorbed Gases," *Ind. Eng. Chem. Fund.*, **13**, 95 (1974).
Gilliland, E.R., R. F. Baddour and J. L. Russel, "Rate of Flow Through Microporous Solids," *AIChE J.*, **4**, 90 (1958).
Halsey, G. D. Jr. and H. S. Taylor, "The Adsorption of Hydrogen on Tungsten Powders," *J. Chem. Phys.*, **15**, 624 (1947).
Higashi, K., H. Ito and J. Oishi, "Surface Diffusion Phenomena in Gaseous Diffusion, (I) Surface Diffusion of Pure Gases," *J. Atomic Energy Soc.*, Japan, **5**, 846 (1963).
Komiyama, H. and J. M. Smith, "Intraparticle Mass Transport in Liquid Filled Pores," *AIChE J.*, **20**, 1110 (1974).
Neretnieks, I., "Adsorption in Finite Bath and Countercurrent Flow with Systems having a Nonlinear Isotherm," *Chem. Eng. Sci.*, **31** 1029 (1976).
Radke, D. J. and J. M. Prausnitz, "Adsorption of Organic Solutes from Dilute Aqueous Solution on Activated Carbon," *Ind. Eng. Chem. Fund.*, **11**, 447 (1972).
Roybal, L. A. and S. I. Sandler, "Surface Diffusion of Adsorbable Gases Through Porous Media," *AIChE J.*, **18**, 39 (1972).
Sudo, Y., D. M. Misic and M. Suzuki, "Concentration Dependence of Effective Surface Diffusion Coefficients in Aqueous Phase Adsorption on Activated Carbon," *Chem. Eng. Sci.*, **33**, 1287 (1978).
Suzuki, M and K. Kawazoe, "Effective Surface Diffusion Coefficients of Volatile Organics on Activated Carbon During Adsorption from Aqueous Solution," *J. Chem. Eng. Japan*, **8**, 379 (1975).
Wicke, E. and R. Kallenbach, "Die Oberflächendiffusion von Kohlendioxyd in aktiven Kohlen," *Kolloid Z.*, **97**, 135 (1941).

Manuscript received May 23, 1980; revision received March 23, and accepted April 23, 1981.

Numerical Solution for the Flow of Highly Viscous Fluid in Agitated Vessel with Anchor Impeller

Fluid motion in an agitated vessel with an anchor impeller is characterized by flow in a horizontal plane induced by the vertical arms of the impeller rotating near the vessel wall. A numerical algorithm of the two-dimensional flow in the horizontal plane is established using an iterative method for the determination of the boundary values of stream function. The computational results of the velocity profiles and agitation power are compared with those of the experiments, and it is shown that the numerical method used in this study is very useful to analyze the flow past the vertical arms of an anchor impeller.

M. KURIYAMA, H. INOMATA, K. ARAI, and S. SAITO

Department of Chemical Engineering
Tohoku University
Sendai, Japan 980

SCOPE

The anchor agitator has a simple and basic configuration suited for agitation of a highly viscous fluid, and is widely used in the chemical and food industries. Analysis of the flow around the vertical blades of an anchor impeller provides significant information on agitation with close-clearance impellers regarding power consumption and mixing and heat transfer performance. Although some experimental studies on flows in the region of anchor impeller blades have been reported (Peters and Smith, 1967, 1969; Murakami et al., 1972), it seems to have been difficult for these experimental studies to give detailed information on flow characteristics such as shear rate distribution, which is usually obtained by differentiating experimental data.

In this respect, numerical study may be significant even if some simplification of a flow field is required to solve a flow problem numerically. However, although laminar, the flow in an anchor-agitated vessel has attracted very few numerical studies. This paucity may mainly be attributed to the existence of plural solid boundaries because while one of the boundary values of the stream function can be prescribed in advance the others must be determined through a computational procedure. Hiraoka et al. (1978) solved numerically two-dimensional flow problems in the horizontal plane of a paddle-agitated vessel with two solid boundaries, i.e., the surfaces of the agitator and of the vessel wall, applying the conservation law of angular momentum. However, no realistic, accurate and stable solution seems yet to have been given for a flow restricted by more than two solid boundaries in a vessel, such as in an anchor-agitated vessel, which has boundaries on the shaft, blades and vessel wall.

Recently, Daiguji and Kobayashi (1979) gave a numerical solution for the two-dimensional flow in channels past two solid bodies and proposed an iterative method for the determination of the boundary values of the stream function by use of the fact

Correspondence concerning this paper should be addressed to S. Saito.
ISSN-0001-1541-82-5582-0385-$2.00.

that the total pressure is a single-valued function of the position in a flow field. This method seems to be useful in the solution of any problems regarding flow restricted by plural solid boundaries.

In the present study, we attempt to apply this method to the analysis of flow behavior in an agitated vessel equipped with an anchor impeller, and the establishment of a computational algorithm of the flow. For the purpose of examining precisely the flow induced by the vertical blades of an anchor impeller, two-dimensional flows in the horizontal plane of the vessel are solved. The computational results of velocity distribution and agitation power are compared with experimental results, and the validity and applicability of this numerical method are discussed. In addition, the shear rate distribution, one of the important numerical results, is demonstrated and its dependence on Reynolds number examined.

CONCLUSIONS AND SIGNIFICANCE

Two-dimensional Newtonian flow problems in the horizontal plane of an agitated vessel with anchor impeller were numerically solved. Taking consideration of the fact that the total pressure is a single-valued function of the position in a flow field, the boundary values of the stream function on the impeller blade and vessel wall respectively were able to be uniquely determined through an iterative procedure. A variation in streamline pattern with a change of Reynolds number was obtained. These patterns agreed qualitatively with the experimental results of Peters and Smith (1967, 1969) and Murakami et al. (1972), and it was found that the mean rotational velocity of the fluid relative to the impeller was affected slightly by Reynolds number and decreased with increasing Reynolds number.

The radial and tangential velocity components and agitation power were also obtained, and then compared with the experimental data obtained from this work and from another paper (Takahashi et al., 1980) for an anchor-agitated vessel. The computational and experimental results were in excellent agreement, and it was shown that the numerical algorithm developed in this work is very useful for the analysis of a flow bounded by plural solid boundaries. Since this algorithm provides a stable method for determining the boundary values of the stream function, it might provide a basis for the derivation of stable solutions for any two-dimensional flows, such as the non-Newtonian flow and the secondary vertical flow in an anchor-agitated vessel insofar as the flows may be expressed by two-dimensional models.

DEVELOPMENT OF EQUATIONS

Governing Equations

Considering the flow past an anchor blade in the horizontal plane of a cylindrical vessel, the domain of the solution is limited to the flow field as shown in Figure 1. Both the impeller blade and the shaft are rotating with angular velocity ω, and the vessel wall is stationary. Newtonian fluid is adopted so as to avoid tedious calculation although non-Newtonian fluid is often encountered in industry. The equation of continuity and the equation of motion for an incompressible Newtonian fluid in a rotating cylindrical coordinate system fixed on an impeller (Greenspan, 1968) are respectively written as follows.

$$\vec{\nabla}^* \cdot \vec{W}^* = 0 \tag{1}$$

$$\vec{W}^*_{t^*} + (\vec{W}^* \cdot \vec{\nabla}^*)\vec{W}^* + \vec{\nabla}^* p^* - \vec{r}^* \vec{\omega}^{*2} + 2\vec{\omega}^* \times \vec{W}^* - \frac{\nu}{R^2\omega}\Delta^* \vec{W}^* = 0 \tag{2}$$

where

$$\vec{W}^* = \vec{W}/R\omega,\ \vec{r}^* = \vec{r}/R,\ \vec{\omega}^* = \vec{\omega}/\omega,\ t^* = t\omega$$

$$p^* = p/\rho R^2\omega^2,\ \vec{\nabla}^* = R\vec{\nabla},\ \Delta^* = R^2\Delta$$

In the above equation, $\vec{W}^*$, $\vec{\omega}^*$, $\vec{r}^*$, and p^* denote the fluid velocity vector, the angular velocity vector, the position vector, and the static pressure, respectively, all which are normalized. And subscript t^* represents the operation of partial differentiation with respect to dimensionless time. With the introduction of the vorticity ζ^* and the stream function ψ^*, Eqs. 1 and 2 can be replaced by the following vorticity equation and Poisson's equation.

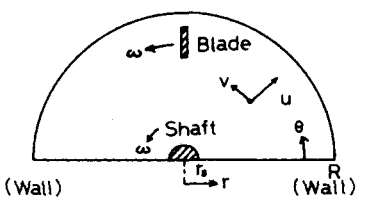

Figure 1. Flow field.

$$\zeta^*_{t^*} + (\vec{W}^* \cdot \vec{\nabla}^*)\zeta^* = \frac{\nu}{R^2\omega}\Delta^*\zeta^* \tag{3}$$

$$\Delta^*\psi^* = 2\omega^* - \zeta^* \tag{4}$$

where ζ^* is relative to the coordinate system fixed on the vessel wall and ψ^* to that fixed on the impeller. From the definition of stream function, the velocity components in the radial and tangential direction, u^* and v^* are given by Eq. 5.

$$u^* = \psi^*_\theta/r^*,\ v^* = -\psi^*_{r^*} \tag{5}$$

where the subscripts, θ and r^* represent the operations of partial differentiation with respect to θ and r^*.

For the convenience of numerical calculation, the flow field as shown in Figure 1 is mapped onto the rectangular mesh system in Figure 2 by using the following transformations.

$$x = ln(r^*/r^*_s),\ y = \theta \tag{6}$$

Then, Eqs. 3, 4, and 5 are rewritten as follows.

$$\zeta^*_{t^*} + \frac{u^*}{r^*}\zeta^*_x + \frac{v^*}{r^*}\zeta^*_y = \frac{\nu}{R^2\omega}\frac{1}{r^{*2}}(\zeta^*_{xx} + \zeta^*_{yy}) \tag{7}$$

$$\psi^*_{xx} + \psi^*_{yy} = r^{*2}(2\omega^* - \zeta^*) \tag{8}$$

$$u^* = \psi^*_y/r^*,\ v^* = -\psi^*_x/r^* \tag{9}$$

where the subscript x or y denotes the operation of partial differentiation with respect to x or y. Equations 7, 8, and 9 should be solved by specifying a suitable set of initial and boundary conditions and stepping the solution out in time until the solution no longer varies significantly with time.

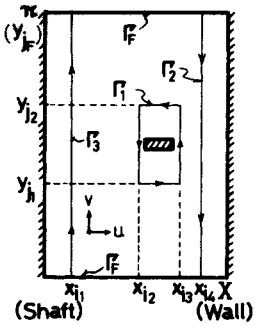

Figure 2. Computational region and integration paths.

Initial and Boundary Conditions

The solution for steady flow is obtained as the asymptotic solution for large time of an unsteady flow. In this work, the following actual initial situation is used as the initial conditions. Fluid, blade, and shaft are initially at rest and then suddenly the blade and shaft begin to rotate with constant angular velocity ω.

The boundary conditions used here are as follows. The flow in the vessel is periodical with a period of π radians in y direction. Namely,

$$\zeta^*, \zeta_y^*, \psi^*, \psi_y^*, u^*, v^*|_{y=0} = \zeta^*, \zeta_y^*, \psi^*, \psi_y^*, u^*, v^*|_{y=\pi} \quad (10)$$

No-slip conditions at the solid surfaces are given by $v^* = -1$, $u^* = 0$ on the vessel wall, and by $v^* = u^* = 0$ on the blade and shaft.

In order to solve Eq. 8, the boundary values of ψ^* are also needed at each computational time step. However, it is impossible to prescribe all the boundary values of ψ^* from the above conditions in advance, and they must be determined through the computational procedure (Daiguji, 1978). In this study, the following method proposed by Daiguji and Kobayashi (1979) may be useful.

The difference in total pressure between points A and B in a flow field can be expressed as the following linear integral.

$$\Delta P^* = P_B^* - P_A^* = -\int_A^B (\vec{W}_{t^*}^* - \vec{W}^* \times \vec{\zeta}^* + \frac{\nu}{R^2\omega}\vec{\nabla}^* \times \vec{\zeta}^*) \cdot d\vec{s} \quad (11)$$

where

$$P^* = p^* + \vec{W}^{*2}/2 - (r^*\omega^*)^2/2$$

In Eq. 11, $\vec{s}$ is the tangent vector to the integration path, and P^* the total pressure. As the total pressure is a single-valued function of the position in a flow field, ΔP^* must be zero whenever a closed integration path is taken. Some numerical solutions for a flow restricted by more than one boundary, however, do not always satisfy this fact. Even though a solution which satisfies some kind of convergence criterion for a steady-state is obtained, it is not a true solution when the pressure residue ΔP^* along a closed path around a solid boundary in a flow field is not zero. This inconsistency of solution often arises from unsuitable resetting of the boundary values of ψ^* during the numerical procedure.

In this work, the ψ^*-value on the shaft is prescribed to be zero and both the values on the blade and vessel wall, ψ_1^* and ψ_2^*, are determined at each computational time step so that both the values of ΔP^* along the closed paths, Γ_1 and Γ_2, around the blade and vessel wall shown in Figure 2 are to be zero by means of the method proposed by Daiguji and Kobayashi (1979).

Equations for Agitation Power

Considering an obstacle laid in a flow field as seen in Figure 3, the torque of the force acting on the obstacle about a fixed point O is evaluated as follows. Multiplying Eq. 2 by the position vector

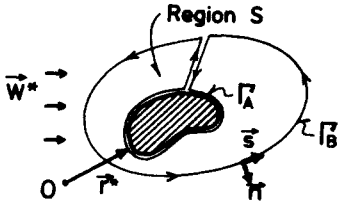

Figure 3. Obstacle in a flow field and integration paths.

$\vec{r}^*$ relative to O and then integrating over the region S enclosed by the path $\Gamma_A + \Gamma_B$ by use of Gauss's divergence theorem, Eq. 12 is obtained.

$$\oint_{\Gamma_A} \{\vec{r}^* \times \vec{n}p^* - \frac{\nu}{R^2\omega}(\vec{n} \cdot \vec{\nabla}^*)(\vec{r}^* \times \vec{W}^*)\}ds = -\iint_S \{\vec{r}^* \times \vec{W}_{t^*}^* + 2\vec{r}^* \times (\vec{\omega}^* \times \vec{W}^*)\}dS - \oint_{\Gamma_B} [(\vec{n} \cdot \vec{W}^*)(\vec{r}^* \times \vec{W}^*) + \vec{r}^* \times \vec{n}p^* - \frac{\nu}{R^2\omega}\{(\vec{n} \cdot \vec{\nabla}^*)(\vec{r}^* \times \vec{W}^*) - 2\vec{n} \times \vec{W}^*\}]ds \quad (12)$$

where $\vec{n}$ is the unit outward normal vector and ds is the line element of the closed path. The left-hand side is the definition for the torque of the force on the obstacle about O itself. Therefore, applying this equation to the present problem, by taking the integration path of Γ_B around the blade and shaft, the torque required to agitate the fluid can be determined as the sum of each calculated value from the right-hand side of Eq. 12.

NUMERICAL METHOD

Finite-Difference Formulas of Governing Equations

The finite-difference method is used to solve the governing equations. The vorticity equation is solved by means of the alternative-direction implicit method improved by Briley (1971) and Poisson's equation by using Crout's method (Akasaka, 1978). Accordingly, Eqs. 7 and 8 are rewritten as the following difference formulas.

Vorticity Equation

$$\frac{\zeta_{i,j}^{*n+1/2} - \zeta_{i,j}^{*n}}{\delta t^*/2} + \frac{u_{i,j}^{*n+1/2}}{r_i^*}(\zeta_x^*)_{i,j}^{n+1/2} + \frac{v_{i,j}^{*n+1/2}}{r_i^*}(\zeta_y^*)_{i,j}^{n} = \frac{\nu}{R^2\omega}\frac{1}{r_i^{*2}}\{(\zeta_{xx}^*)_{i,j}^{n+1/2} + (\zeta_{yy}^*)_{i,j}^{n}\} \quad (13)$$

$$\frac{\zeta_{i,j}^{*n+1} - \zeta_{i,j}^{*n+1/2}}{\delta t^*/2} + \frac{u_{i,j}^{*n+1/2}}{r_i^*}(\zeta_x^*)_{i,j}^{n+1/2} + \frac{v_{i,j}^{*n+1/2}}{r_i^*}(\zeta_y^*)_{i,j}^{n+1} = \frac{\nu}{R^2\omega}\frac{1}{r_i^{*2}}\{(\zeta_{xx}^*)_{i,j}^{n+1/2} + (\zeta_{yy}^*)_{i,j}^{n+1}\} \quad (14)$$

Poisson's Equation

$$(\psi_{xx}^*)_{i,j}^{n+1} + (\psi_{yy}^*)_{i,j}^{n+1} = r_i^{*2}(2\omega^* - \zeta_{i,j}^{*n+1}) \quad (15)$$

In the above equations, the subscripts i, j correspond to the x, y-coordinates, and the superscript n is the time step index. The derivatives in Eqs. 13, 14 and 15 can be expressed by use of a nonuniform mesh system. The expressions for x-direction are

$$(f_x)_{i,j} = \frac{1}{\delta x_i + \delta x_{i-1}}\left\{\frac{\delta x_{i-1}}{\delta x_i}(f_{i+1,j} - f_{i,j}) - \frac{\delta x_i}{\delta x_{i-1}}(f_{i-1,j} - f_{i,j})\right\} \quad (16)$$

$$(f_{xx})_{i,j} = \frac{2}{\delta x_i + \delta x_{i-1}}\left\{\frac{1}{\delta x_i}(f_{i+1,j} - f_{i,j}) + \frac{1}{\delta x_{i-1}}(f_{i-1,j} - f_{i,j})\right\} \quad (17)$$

where f represents ζ^* or ψ^* and δx_i is defined by $\delta x_i = x_{i+1} - x_i$. The same expressions are also obtained for y-direction.

Modification of Boundary Values of Stream Function

Equation 11 can be transformed into the difference form for the residual values of the total pressure along the closed paths, Γ_1 and Γ_2, as follows.

$$\Delta P_1^{*n+1/2} = -\sum_{i=i_2+1}^{i_3}\left[\left(r^*u_{i^*}^* - r^*v^*\zeta^* + \frac{\nu}{R^2\omega}\zeta_y^*\right)_{i-1/2,j_1}^{n+1/2} - \left(r^*u_{i^*}^* - r^*v^*\zeta^* + \frac{\nu}{R^2\omega}\zeta_y^*\right)_{i-1/2,j_2}^{n+1/2}\right]\cdot\delta x_{i-1} + \sum_{j=j_1+1}^{j_2}\left[\left(r^*v_{i^*}^* + r^*u^*\zeta^* - \frac{\nu}{R^2\omega}\zeta_x^*\right)_{i_2,j-1/2}^{n+1/2} - \left(r^*v_{i^*}^* + r^*u^*\zeta^* - \frac{\nu}{R^2\omega}\zeta_x^*\right)_{i_3,j-1/2}^{n+1/2}\right]\cdot\delta y_{j-1} \quad (18)$$

$$\Delta P_2^{*n+1/2} = 2\sum_{j=2}^{j_E}\left[\left(r^*v_{i^*}^* + r^*u^*\zeta^* - \frac{\nu}{R^2\omega}\zeta_x^*\right)_{i_4,j-1/2}^{n+1/2}\right]\cdot\delta y_{j-1} \quad (19)$$

Corresponding to the magnitudes of these pressure residues, the boundary values of ψ_1^* and ψ_2^* are improved by the following equations proposed by Daiguji and Kobayashi (1979) in an iterative procedure at each computational time step.

$$\psi_\mu^{*(N+1)} = \psi_\mu^{*(N)} + \alpha\Delta\psi^{*(N+1)} \quad (20)$$

$$\sum_{\mu=1}^{M} I_{\mu,\nu}\cdot\Delta\psi_\mu^{*(N+1)} = \Delta P_\nu^{*n+1/2(N)}\cdot\delta t^* \quad (21)$$

$$(\nu = 1,2,\ldots M)$$

In the above equations, M denotes the number of solid boundaries, the superscript N is the iteration index, ψ_μ^* is the stream function on the μ-th obstacle to be improved by the correction factor $\Delta\psi_\mu^*$, ΔP_ν^* is the pressure residue along the path Γ_ν, and α is a constant limited from 0 to 1, which is chosen to accelerate the convergence of solution. $I_{\mu,\nu}$ in Eq. 21 is the value of circulation along the path Γ_ν, which is obtained by taking the stream function on the μ-th obstacle as unity and those on others as zero. Namely, $I_{\mu,\nu}$ is expressed as

$$I_{\mu,\nu} = -\oint_{\Gamma_\nu}\left(\frac{\partial\psi^*}{\partial n}\right)ds \quad (22)$$

where ds is the line element of the path Γ_ν, and $\partial/\partial n$ denotes the operation of partial differentiation with respect to the outward direction normal to Γ_ν. ψ^* in Eq. 22 is given as a solution of

$$\psi_{xx}^* + \psi_{yy}^* = 0 \quad (23)$$

In this work, we designate the blade as the 1st obstacle and the vessel wall as the 2nd one. For example, $I_{1,1}$ and $I_{1,2}$ can be obtained under the boundary conditions of $\psi^* = 1$ on the 1st obstacle and $\psi^* = 0$ on the 2nd one. In addition to these conditions, the periodic condition of $\psi^*, \psi_y^*|_{y=0} = \psi^*, \psi_y^*|_{y=\pi}$ is needed.

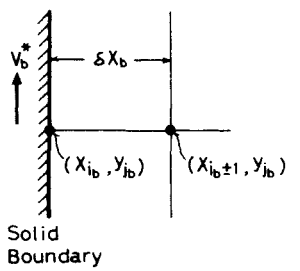

Figure 4. Notation for grid points near the solid boundary.

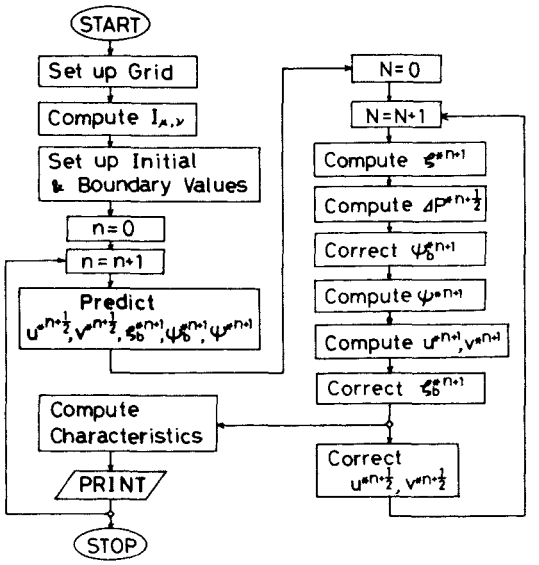

Figure 5. Computational procedure.

Determination of Boundary Vorticities

The expressions for the boundary vorticities are derived to satisfy the no-slip condition. We consider a solid boundary parallel to the y-axis, moving in the y-direction with speed v_b^* as seen in Figure 4. Through the expansion of the stream function in Taylor series, the following expression is obtained by eliminating the higher order derivatives than the fourth, and by substituting the lower ones from the first to the third for vorticity and velocity using Eqs. 8 and 9.

$$\zeta_{ib,jb}^* = \frac{1}{1\pm\delta x_b}\left\{-\frac{1}{2}\zeta_{ib\pm1,jb}^* + 3\omega^* \pm 2\delta x_b - \frac{3}{r_{ib}^{*2}\cdot\delta x_b^2}(\psi_{ib\pm1,jb}^* - \psi_{ib,jb}^*) \mp \frac{3v_b^*}{r_{ib}^*\cdot\delta x_b}\right\} \quad (24)$$

Similarly, the velocity at a boundary parallel to the x-axis, moving with speed u_b^* (in this work, $u_b^* = 0$), is given as

$$\zeta_{ib,jb}^* = -\frac{1}{2}\zeta_{ib,jb\pm1}^* + 3\omega^* - \frac{3}{r_{ib}^{*2}\cdot\delta y_b^2}(\psi_{ib,jb\pm1}^* - \psi_{ib,jb}^*) \pm \frac{3u_b^*}{r_{ib}^*\cdot\delta y_b} \quad (25)$$

To apply Eqs. 24 and 25 to evaluate the vorticities on the blade, the values at convex corners are approximated by the arithmetic mean of the vorticities from Eqs. 24 and 25.

Computational Scheme

The outline of computational procedure is illustrated by the flow chart in Figure 5. In this figure, the variables of which the sub-

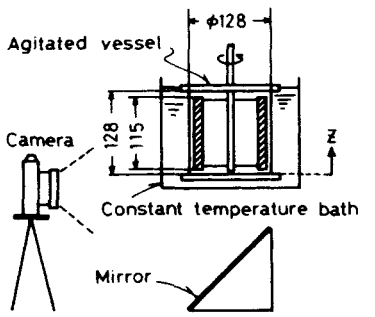

Figure 6. Schematic diagram of experimental apparatus.

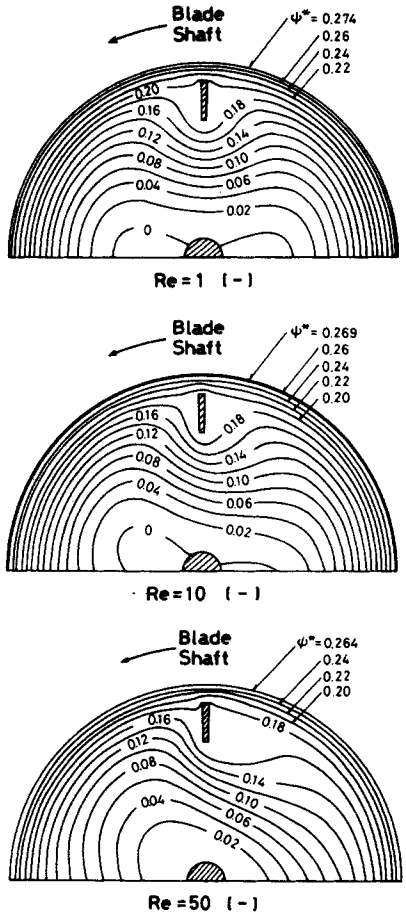

Figure 7. Stream lines drawn relative to the blade.

scripts are omitted are ones at interior points, while the boundary values are represented by the subscript b. A summary is now given of the algorithm which was used to advance the time-dependent variables from the n-th to the $(n+1)$-th time level.

1) Predict $u^{*n+1/2}$, $v^{*n+1/2}$, ζ_b^{*n+1}, ψ_b^{*n+1} and ψ^{*n+1} by a linear extrapolation from the n-th and $(n-1)$-th time levels. At $n = 1$, this procedure is omitted and those values are replaced by the initial values at $n = 0$.

2) Solve Eqs. 13 and 14 to obtain the new ζ^{*n+1}.

3) Compute the pressure residues along the paths, Γ_1 and Γ_2 using the new ζ^{*n+1} and the last values of ψ^{*n+1}, $u^{*n+1/2}$ and $v^{*n+1/2}$.

4) Correct ψ_b^{*n+1} using Eqs. 20 and 21.

5) Solve Eq. 15 to obtain the new ψ^{*n+1}.

6) Compute u^{*n+1} and v^{*n+1} using the new ψ^{*n+1} from Eq. 9.

7) Correct ζ_b^{*n+1} using Eqs. 24 and 25.

8) If the pressure residues obtained at step 3) are less than the desired criterion, the calculation is advanced to the new time level increased by increment δt^*. If not, $u^{*n+1/2}$ and $v^{*n+1/2}$ are re-evaluated and the calculation is returned to step 2).

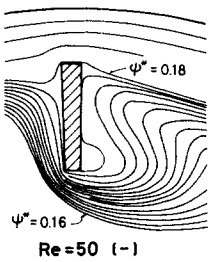

Figure 8. Flow near the blade.

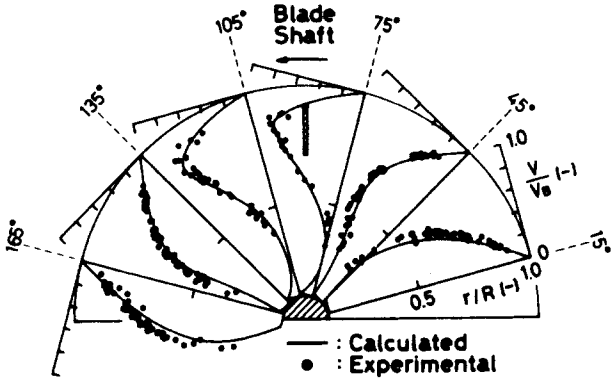

Figure 9. Tangential velocity distributions (Re = 1).

The above computational cycle is repeated until a steady-state solution is obtained.

The torque required to agitate the fluid is evaluated at the $(n+1/2)$-th time step as the sum of $T_B^{*n+1/2}$, the torque of the force on the blade, and $T_S^{*n+1/2}$, that on the shaft, from the following difference equations which are derived from Eq. 12.

$$
\begin{aligned}
T_B^{*n+1/2} = \sum_{i=i_2+1}^{i_3} \Bigg[\Bigg\{ & r^{*2}v^{*2} + r^{*2}p^* - \frac{\nu}{R^2\omega} r^*(v_y^* + 2u^*) \\
& + 2r^{*2}\omega^*\psi^* \Bigg\}_{i-1/2,j_2}^{n+1/2} \\
& - \Bigg\{ r^{*2}v^{*2} + r^{*2}p^* - \frac{\nu}{R^2\omega} r^*(v_y^* + 2u^*) \\
& + 2r^{*2}\omega^*\psi^* \Bigg\}_{i-1/2,j_1}^{n+1/2} \Bigg] \cdot \delta x_{i-1} \\
& + \sum_{j=j_1+1}^{j_2} \Bigg[\Bigg\{ r^{*2}u^*v^* - \frac{\nu}{R^2\omega} r^*(v_x^* - v^*) \Bigg\}_{i_3,j-1/2}^{n+1/2} \\
& - \Bigg\{ r^{*2}u^*v^* - \frac{\nu}{R^2\omega} r^*(v_x^* - v^*) \Bigg\}_{i_2,j-1/2}^{n+1/2} \Bigg] \cdot \delta y_{j-1} \\
& + \sum_{j=j_1+1}^{j_2} \Bigg[\sum_{i=i_2+1}^{i_3} \left\{ \frac{(v^{*n+1} - v^{*n})r^{*3}}{\delta t^*} \right\}_{i-1/2,j-1} \cdot \delta x_{i-1} \\
& + \sum_{i=i_2+1}^{i_3} \left\{ \frac{(v^{*n+1} - v^{*n})r^{*3}}{\delta t^*} \right\}_{i-1/2,j} \cdot \delta x_{i-1} \Bigg] \cdot \frac{1}{2} \delta y_{j-1} \qquad (26)
\end{aligned}
$$

$$
\begin{aligned}
T_S^{*n+1/2} = & \sum_{j=2}^{j_F} \left\{ r^{*2}u^*v^* - \frac{\nu}{R^2\omega} r^*(v_x^* - v^*) \right\}_{i_1,j-1/2}^{n+1/2} \cdot \delta y_{j-1} \\
& + \sum_{j=2}^{j_F} \Bigg[\sum_{i=2}^{i_1} \left\{ \frac{(v^{*n+1} - v^{*n})r^{*3}}{\delta t^*} \right\}_{i-1/2,j-1} \cdot \delta x_{i-1} \\
& + \sum_{i=2}^{i_1} \left\{ \frac{(v^{*n+1} - v^{*n})r^{*3}}{\delta t^*} \right\}_{i-1/2,j} \cdot \delta x_{i-1} \Bigg] \cdot \frac{1}{2} \delta y_{j-1} \qquad (27)
\end{aligned}
$$

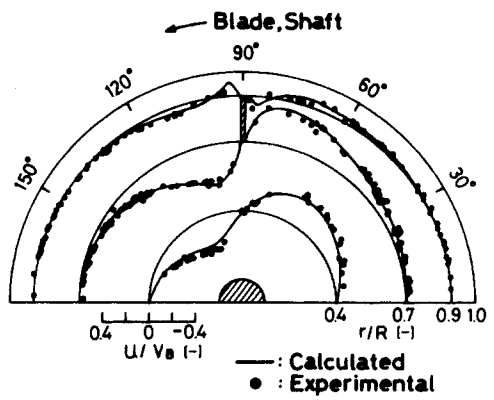

Figure 10. Radial velocity distributions (Re = 1).

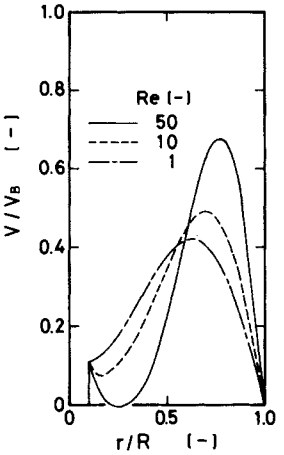

Figure 11. Typical variation in the tangential velocity distribution with the change of Reynolds number.

where the subscripts i_1, i_2, i_3, j_1, j_2, and j_F represent the x, y-coordinates as shown in Figure 2.

EXPERIMENTAL

Velocity profiles in an agitated vessel equipped with an anchor impeller were measured and compared with the computational results. The experimental apparatus is shown in Figure 6, schematically. The cylindrical vessel, which was made of transparent acrylic resin, had a flat lid and a flat bottom. The vessel was immersed in water in a square-sided transparent acrylic vessel to reduce optical distortions. The impeller was the same anchor impeller as used by Takahashi et al. (1980), i.e., a close-clearance type impeller which consisted of two vertical flat plates. An aqueous solution of corn syrup known as a Newtonian fluid was used. Small solid particles of almost the same density as the agitated fluid were used to trace the motions of the fluid. The local velocities of the fluid were determined by analyzing photographs of the side view and bottom view of the agitated vessel.

In addition, the agitation power for the impeller was measured by a rotating torque meter and compared with the computational results.

RESULTS AND DISCUSSION

Numerical analysis was carried out for the case of clearance ratio $c/D = 0.05$, as an example. Both the width of the blade and the diameter of the shaft are one-tenth of the vessel diameter.

Flow Patterns

The variation in streamline pattern with increasing Reynolds number is illustrated in Figure 7, and an example of the flow near the impeller blade is shown in Figure 8 in detail. These patterns show tendencies similar to those of the experimental results reported by Peters and Smith (1967, 1969) and Murakami et al. (1972). Namely, with increasing Reynolds number, the symmetry evidence of the flow respect to the blade is gradually lost, and at Re = 50, a region where the fluid moves with the blade is seen behind the blade as shown in Figure 8. Both the ψ^*-values on the blade and vessel wall decrease slightly with increasing Reynolds number, which means that the average rotational velocity of the fluid relative to the impeller is affected slightly by Reynolds number and decreases with increasing Reynolds number.

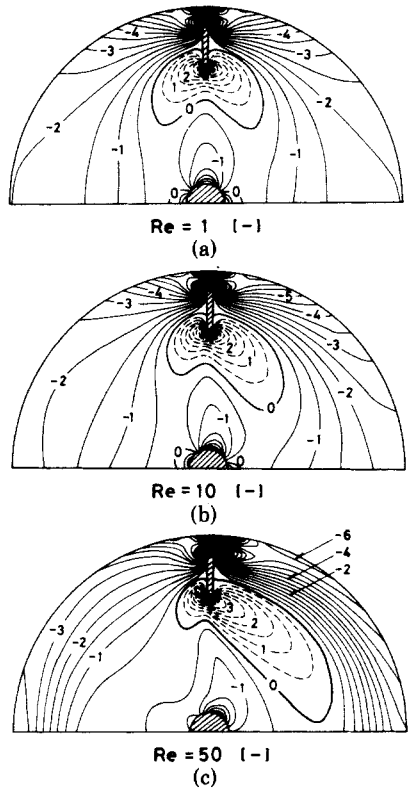

Figure 13. Distributions of shear rate, $\partial(v/R\omega)/\partial(r/R)$, all over the flow field.

Velocity and Shear Rate Distributions

Typical distributions of fluid velocities relative to the coordinate system fixed on the vessel wall are shown in Figures 9 and 10, in which v_B is the tangential velocity of the outer-tip of the blade. Figure 9 shows the tangential velocity distributions at $\theta = 15°$, 45°, 75°, 105°, 135°, and 165°, and Figure 10 the radial ones at $r/R = 0.4$, 0.7, and 0.9. The experimental values plotted in these figures were measured in the region of $0.5 \leqq z/D \leqq 0.8$. Excellent agreements between the calculated and observed profiles were obtained all over the flow field.

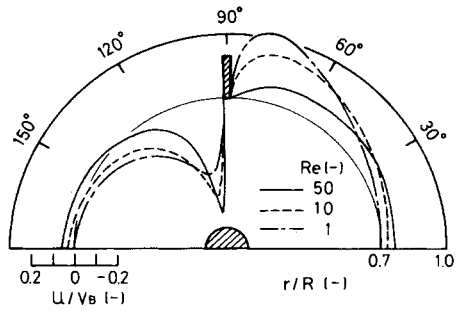

Figure 12. Typical variation in the radial velocity distribution with the change of Reynolds number.

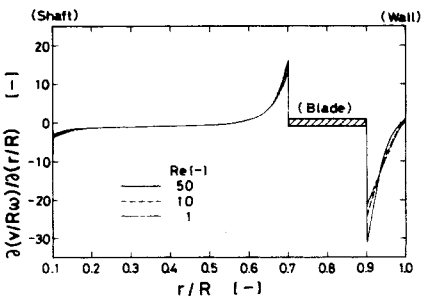

Figure 14. Shear rate distributions along radial direction.

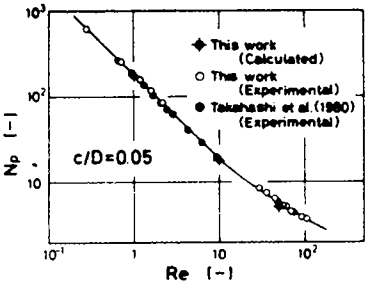

Figure 15. Correlation of agitation power.

Typical variations in tangential and radial velocity distributions with the change of Reynolds number are shown in Figures 11 and 12, respectively. Figure 11 shows the downstream velocity distributions at 45° from the blade. With increasing Reynolds number, the fluid drag by the impeller blade is greater, thus the distribution curve has a larger maximum value. Figure 12 shows the radial velocity distributions at $r/R = 0.7$. The fluid is displaced in toward the shaft and passes around behind the blade. The displacement flow which appears immediately in front of the blade is more remarkable at higher Reynolds number, while the flow around behind the blade is more pronounced at lower Reynolds number.

The shear rate distribution is also calculated. Figures 13(a) to 13(c) show the distributions of normalized tangential shear rate, $\partial(v/R\omega)/\partial(r/R)$, relative to the coordinate system fixed on the blade. It is evident that high shear rate appears near the inner and the outer edges of the blade. However, the shear rate becomes suddenly small in the region apart from the blade. Although the pattern of the distribution changes with increasing Reynolds number, the degree of non-uniformity in normalized shear rate in the flow field is relatively unaffected by Reynolds number. The detailed distributions along radius at the blade position are shown in Figure 14. The distribution curves are similar to those reported by Peters and Smith (1967). From this figure, it can be seen that the difference among the normalized curves at each Reynolds number is enhanced at the regions near the solid boundaries, especially at the clearance between the blade and the vessel wall, where considerable variation in the shear rate is observed.

Agitation Power

The calculated results of steady-state torque are compared with the experimental data obtained from this work and from another paper (Takahashi et al., 1980) in Figure 15, plotting power number, N_p, versus Reynolds number, Re. It is evident that the computational and experimental results are quite well in agreement. These calculated values are independent of the choice of closed integration paths around the blade and shaft.

ACKNOWLEDGMENT

The authors wish to express their appreciation to Dr. Hisaaki Daiguji for numerous discussions and helpful comments.

NOTATION

c	= clearance between blade-tip and vessel wall
D	= vessel diameter
d	= impeller diameter
N	= rotational speed of impeller
N_p	= power number ($= 2\pi T/\rho N^2 d^5$)
$\vec{n}$	= unit vector normal to closed path
$\partial/\partial n$	= partial differentiation with respect to normal direction to closed path
P,p	= total or static pressure
ΔP	= pressure residue defined in Eq. 11
R	= vessel radius
Re	= Reynolds number ($= d^2N/\nu$)
$\vec{r}$	= position vector
r_S	= shaft radius
r,θ	= cylindrical coordinates
S	= surface area shown in Figure 3
$\vec{s}$	= tangent vector along closed path
T	= torque required to agitate fluid
T_B,T_S	= torques of the forces on the blade and the shaft
t	= time
δt	= time space
u,v	= velocity components
v_B	= tangential velocity of blade-tip
$\vec{W}$	= velocity vector
x,y	= rectangular coordinates
$\delta x,\delta y$	= grid spaces
z	= axial distance from vessel bottom

Greek Letters

Γ	= closed path
Δ	= Laplacian
$\vec{\nabla}$	= vector operator known as nabla
$\vec{\zeta}$	= vorticity vector
ζ	= vorticity
μ	= viscosity
ν	= kinematic viscosity
λp	= density
ψ	= stream function
$\vec{\omega}$	= angular velocity vector
ω	= angular velocity

Subscripts

$A,B,F,1,2,3$	= closed path indexes in Figures 2 and 3
b	= boundary value
i,j	= i-th row and j-th column
x,y,r,θ,t	= partial differentiation with respect to x, y, r, θ, and t, respectively
μ	= μ-th obstacle
ν	= ν-th closed path

Superscripts

N	= N-th approximation
n	= n-th time step
*	= dimensionless variable

LITERATURE CITED

Akasaka, T., *Numerical Computation* (in Japanese), Corona Publishing Co. Ltd., Tokyo (1978).

Briley, W. R., "Numerical Study of Laminar Separation Bubbles Using the Navier-Stokes Equations," *J. Fluid Mech.*, **47**, 713 (1971).

Daiguji, H., "Numerical Solution for the Time-Dependent Two-Dimensional Viscous Flows past Obstacle (Part 1, Channel Flow with an Oscillating Plate (in Japanese)," *Bull. JSME*, **44**, 555 (1978).

———, and S. Kobayashi, "Numerical Solution for the Time-Dependent Two-Dimensional Viscous Flows past Obstacle (Part 3, Channel Flow past Plural Regular Prisms) (in Japanese)," Preprint of JSME, No. 793-7, 18 (1979).

Greenspan, H. P., *The Theory of Rotating Fluids*, Cambridge University Press (1968).

Hiraoka, S., I. Yamada, and K. Mizoguchi, "Numerical Analysis of Flow Behavior of Highly Viscous Fluid in Agitated Vessel," *J. Chem. Eng. Japan*, **11**, 487 (1978).

Murakami, Y., K. Fujimoto, T. Shimada, A. Yamada, and K. Asano, "Evaluation of Performance of Mixing Apparatus for High Viscosity Fluids," *J. Chem. Eng. Japan*, **5**, 297 (1972).

Peters, D. C., and J. M. Smith, "Fluid Flow in the Region of Anchor Agitator Blades," *Trans. Instn. Chem. Engrs.*, **45**, T360 (1967).

———, "Mixing in Anchor Agitated Vessel," *Can. J. Chem. Eng.*, **47**, 268 (1969).

Takahashi, K., K. Arai, and S. Saito, "Power Correlation for Anchor and Helical Ribbon Impellers in Highly Viscous Liquids," *J. Chem. Eng.*, Japan, **13**, 147 (1980).

Manuscript received October 13, 1980; revision received June 18 and accepted July 14, 1981.